Precambrian Research 397 (2023) 107200

Contents lists available at ScienceDirect

Precambrian Research

journal homepage: www.elsevier.com/locate/precamres

Initial cyclostratigraphy of the middle Nama Group (Schwarzrand Subgroup) in southern Namibia

Bianca R. Spiering [a,*], Ajani Bissick [b], Simon A.F. Darroch [c,d], Joshua H.F.L. Davies [e], Brandt M. Gibson [c,f], Galen P. Halverson [b], Marc Laflamme [f], Frederik J. Hilgen [a]

[a] Department of Earth Sciences, Faculty of Geosciences, Utrecht University, Utrecht 3584 CB, The Netherlands
[b] Department of Earth and Planetary Sciences/Geotop, McGill University, Montréal, QC H3A 0E8, Canada
[c] Department of Earth and Environmental Sciences, Vanderbilt University, Nashville, TN 37235-1805, USA
[d] Senckenberg Research Institute and Museum of Natural History, Frankfurt 60325, Germany
[e] Département des Sciences de la Terre et de l'Atmosphère/Geotop, Université du Québec à Montréal, Montréal, QC H3C 3P8, Canada
[f] Department of Chemical and Physical Sciences, University of Toronto Mississauga, Mississauga, ON L5L 1C6, Canada

ARTICLE INFO

Keywords:
Ediacaran
Nama Group
Cyclostratigraphy
Astronomical climate forcing
Milankovitch cycles

ABSTRACT

The Ediacaran Period includes critical evolutionary trends of early complex life as well as climatic variations associated with ocean oxygenation, glaciations, and carbon cycling, which are still poorly understood in terms of astronomical climate forcing. The middle Nama Group in southern Namibia was deposited during the late Ediacaran in mainly shallow marine environments within a foreland basin and consists of hierarchically arranged depositional sequences. Here, we test a possible astronomical origin of these sedimentary variations by developing an initial cyclostratigraphic framework based on satellite images integrated with recently published high-precision U-Pb zircon ages. Regular sedimentary alternations occur dominantly on scales of several tens of meters, accompanied by smaller- and larger-scale variations, and are correlatable over distances of ~50 km. Throughout the studied succession, 35 to 39 alternations are recognized on this dominant scale, which have an average duration of ~120–180 k.y. This duration corresponds well with the period of short eccentricity (~100 k.y.), given the likely presence of hiatuses, or alternatively, the period of obliquity amplitude modulation (~173 k.y.), which would imply no time is missing on this scale. The dominant alternations are consistent with previously identified medium-scale sequences in this succession, which have been interpreted to record fluctuations in relative or eustatic sea level. We hypothesize that astronomically-forced fluctuations in eustatic sea level modulated deposition of the middle Nama Group. Geochemical studies suggested a relation between fossil distribution, redox variability and sea level, implying that astronomical forcing may have played a role in the distribution of early complex life.

1. Introduction

The Ediacaran Period (635–538 Ma; Xiao and Narbonne, 2020) marks a critical interval in the evolution of life on Earth: the emergence of the Ediacara biota ~574 Ma (Matthews et al., 2021), the first complex macroscopic organisms, and their extinction around the Ediacaran-Cambrian boundary, after which most modern metazoan phyla diversified during the Cambrian Explosion of Life (Erwin et al., 2011). Geochemical data indicate dynamic ocean redox conditions during this interval (e.g., Li et al., 2020; Tostevin and Mills, 2020; Wei et al., 2021), possibly linked to phases of metazoan radiation (Wood et al., 2019). Besides the iconic Gaskiers glaciation at ~580 Ma (Pu et al., 2016), other, possibly more regional, glaciations have been proposed for the late Ediacaran (e.g., Chumakov, 2011; Linnemann et al., 2022). Additionally, significant shifts in carbon isotopic composition are recognized in carbonate strata, including the Shuram excursion during which values drop to −12‰ or lower (Burns and Matter, 1993; Grotzinger et al., 2011; Wang et al., 2014). However, the role that astronomical climate forcing played in such events is still poorly understood for the late Ediacaran, even though it has been recognized as a significant driver of Earth's

* Corresponding author at: Princetonlaan 8a, 3584 CB Utrecht, The Netherlands.
E-mail addresses: b.r.spiering@uu.nl (B.R. Spiering), ajani.bissick@mail.mcgill.ca (A. Bissick), simon.a.darroch@vanderbilt.edu (S.A.F. Darroch), davies.joshua@uqam.ca (J. H.F.L. Davies), brandt.gibson@utoronto.ca (B.M. Gibson), galen.halverson@mcgill.ca (G.P. Halverson), marc.laflamme@utoronto.ca (M. Laflamme), f.j.hilgen@uu.nl (F.J. Hilgen).

https://doi.org/10.1016/j.precamres.2023.107200
Received 1 June 2023; Received in revised form 24 August 2023; Accepted 23 September 2023
Available online 29 September 2023

climate throughout the Phanerozoic Eon and older parts of the Precambrian (Hinnov, 2013; Lantink et al., 2023), including the middle Ediacaran (e.g., Gong and Li, 2020).

The Nama Group in southern Namibia includes a late Ediacaran succession of mixed carbonate-siliciclastic rocks (Germs, 1983; Saylor et al., 1995), which displays hierarchical stacking patterns (Saylor, 2003), potentially indicative of an astronomical origin. Deposition occurred in fluvial to marine slope environments of a foreland basin that developed between the Kalahari Craton and the Damara and Gariep orogenic belts (Blanco et al., 2011; Germs, 1983; Gresse and Germs, 1993). Saylor (2003) developed a sequence stratigraphic framework consisting of a hierarchy of three scales of depositional sequences. Even though some of the large-scale sequences were linked to tectonism, a eustatic (climatic) origin has yet to be investigated for the other large-, medium-, and small-scale sequences (Saylor, 2003). The potential role of astronomical climate forcing can be independently tested using high-precision U-Pb ages of zircons from volcanic ash beds. Until recentlty, this was not possible due to ages with large uncertainties relative to the scale of astronomical cycles (~1 m.y.; Grotzinger et al., 1995). However, recent techniques yield extremely precise dates with uncertainties of 0.1–0.3 m.y. (Linnemann et al., 2019; Nelson et al., 2022), which have not yet been used to test a possible astronomical origin for the depositional sequences.

Here, we develop an initial cyclostratigraphic framework for the Nama Group in the Witputs subbasin using satellite images (Google Earth) integrated with the recently published high-precision U-Pb zircon ages (Linnemann et al., 2019; Nelson et al., 2022), which provides detailed stratigraphic correlations and estimates of the durations of the sedimentary variations. This will allow for the integration of sequence stratigraphy, geochemistry, and biotic distribution and diversity (as expressed by both trace and body fossils) to investigate the relationship between astronomical forcing, sea level, redox state, and biota during the late Ediacaran in southern Namibia. This effort will complement ongoing research focused on the late Ediacaran and the transition to the Cambrian by, for example, the Geological Research through Integrated Neoproterozoic Drilling (GRIND) project (e.g., Rose et al., 2023).

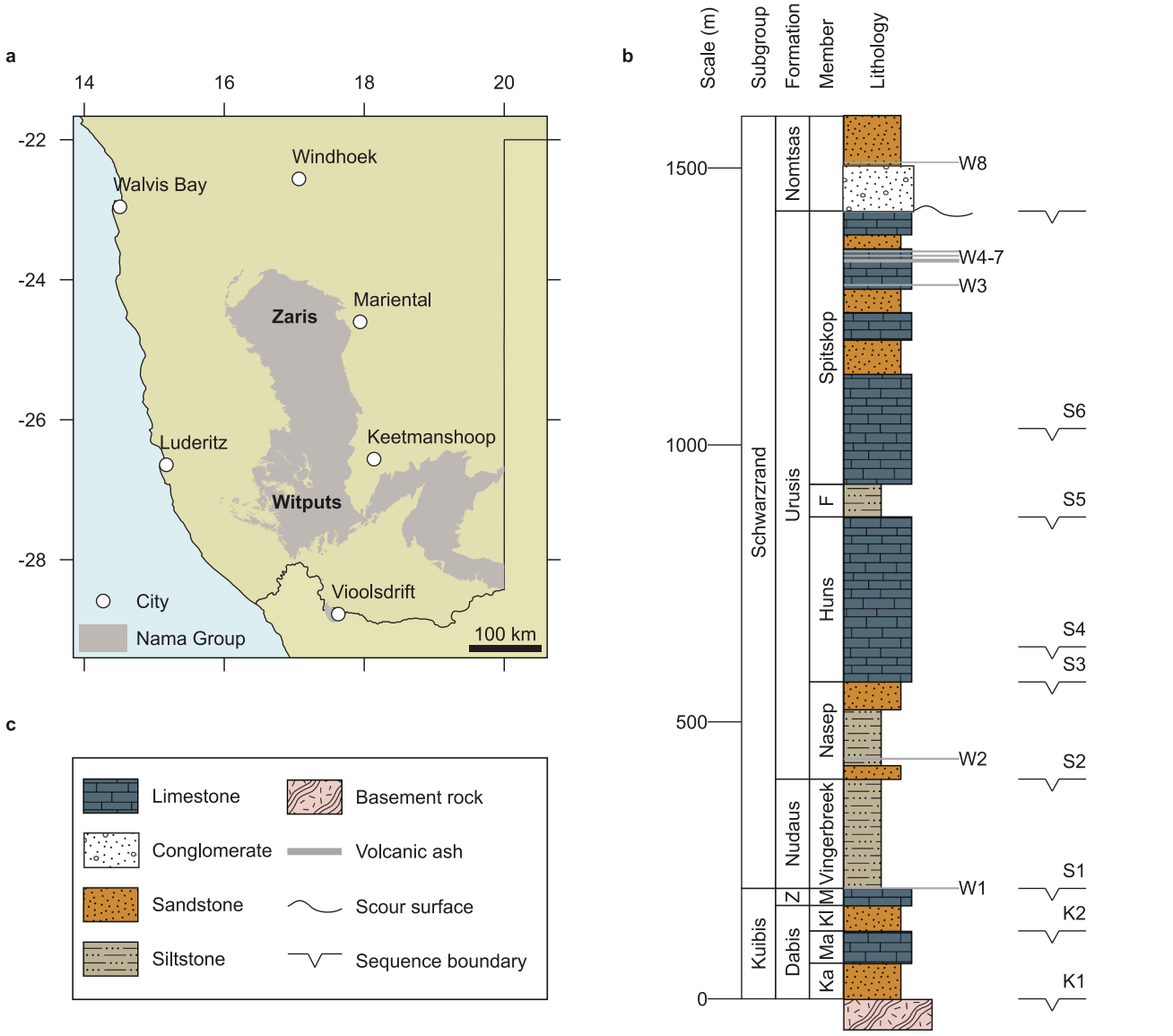

Fig. 1. (a) Map of southern Namibia showing the outcrop area of the Nama Group and the positions of the Zaris and Witputs subbasins. (b) General stratigraphic column of the lower and middle Nama Group in the Witputs subbasin adapted from Nelson et al. (2022) with large-scale depositional sequences after Saylor et al. (1995) and Saylor (2003). F = Feldschuhhorn, Ka = Kanies, Kl = Kliphoek, M = Mooifontein, Ma = Mara, Z = Zaris. (c) Legend to b.

2. Geological setting

2.1. Geodynamic setting

The Nama foreland basin is located on the western margin of the Kalahari Craton and is flanked by the central Damara and Gariep orogenic belts to the north and west, respectively (Blanco et al., 2011; Gresse and Germs, 1993). These belts formed during the late Neoproterozoic and early Cambrian due to collision between the Kalahari, Congo and Río de la Plata Cratons during the assembly of western Gondwana (Blanco et al., 2011; Gray et al., 2008). Reconstructions of global paleogeography indicate that the Kalahari Craton was located between 40 and 60°S at ~540 Ma (Li et al., 2013).

The Nama Basin is subdivided into the northern Zaris and southern Witputs subbasins (Fig. 1a), which were separated by the east–west trending Osis Ridge (Gresse and Germs, 1993). This ridge probably represented a forebulge (Germs and Gresse, 1991) that mainly influenced sedimentation of the lower Nama Group (Germs, 1983). The Nama Group extends into the Vioolsdrift area in the northwest of the Republic of South Africa (Germs and Gresse, 1991; Nelson et al., 2022), which could be a separate subbasin (Germs and Gresse, 1991) or a part of the Witputs subbasin (Germs et al., 2009).

2.2. Lithostratigraphy

In ascending order, the Nama Group consists of the Kuibis, Schwarzrand and Fish River Subgroups (Germs, 1983). In the Witputs subbasin, the Kuibis Subgroup contains two successions with a siliciclastic-dominated lower part and carbonate-dominated upper part (Germs, 1983; Fig. 1b). The Schwarzrand Subgroup is subdivided into the Nudaus, Urusis, and Nomtsas Formations (Fig. 1b). The Nudaus Formation mostly consists of red and green shale with interspersed sandstone beds (Saylor et al., 1995). The Urusis Formation is further subdivided into the Nasep, Huns, Feldschuhhorn, and Spitskop Members. The Nasep Member is mainly composed of sand- and siltstones, including a distinct, thick-bedded sandstone unit at its base (Saylor et al., 1995). This is overlain by carbonate deposits of the Huns and Spitskop Members, separated by a green siltstone-dominated interval comprising the Feldschuhhorn Member (Saylor et al., 1995). The Urusis and Nomtsas Formations are separated by an erosional disconformity with incised valleys that are filled by conglomerates and siltstones (Saylor et al., 1995). In the Vioolsdrift area, however, no unconformity is found at this formation boundary (Nelson et al., 2022). The overlying Fish River Subgroup consists mainly of reddish sandstones (Germs, 1983).

2.3. Biostratigraphy

Ediacaran fossils have been found throughout the Kuibis and Schwarzrand Subgroups (Germs, 1983; Grotzinger et al., 1995). The oldest occurrences of soft-bodied Ediacara biota in Namibia, consisting of assemblages of *Ernietta*, were found in sediments at Farm Hansburg, which were initially interpreted as Kanies Member (Bouougri et al., 2011) but reinterpreted as Kliphoek Member of the Dabis Formation in the Kuibis Subgroup (Maloney et al., 2020). The latter unit also contains the oldest trace fossils, consisting of simple plug-shaped burrows (Cribb et al., 2019). The upper Kliphoek Member at Farm Aar, redefined as Aar Member (Hall et al., 2013), hosts a diverse assemblage of Ediacaran fossils, including *Rangea*, *Ernietta*, and *Pteridinium* (Vickers-Rich et al., 2013). Ediacara biota, as well as skeletal metazoan fossils like *Cloudina*, range upwards from the Kuibis Subgroup to the upper Spitskop Member at Farm Swartpunt (Darroch et al., 2015; Grotzinger et al., 1995; Narbonne et al., 1997). Throughout this succession, trace fossils indicate a generalized trend of increased diversity and behavioral complexity (Cribb et al., 2019; Darroch et al., 2021). Abundant and well-preserved specimens of the complex trace fossil *Treptichnus pedum* (formerly *Phycodes pedum*) were found in the Nomtsas Formation at Farm Sonntagsbrunn (Grotzinger et al., 1995; Wilson et al., 2012). This indicates that the Ediacaran-Cambrian boundary, as defined by the lowest occurrence of *Treptichnus pedum* (Brasier et al., 1994), is located near or within the disconformity between the Spitskop Member and Nomtsas Formation (Grotzinger et al., 1995; Linnemann et al., 2019).

2.4. Sequence stratigraphy

Strata of the Urusis Formation in the Witputs subbasin were deposited in three paleogeographic zones from east to west: landward margin, depocenter, and seaward margin (Saylor, 2003). Siliciclastic facies associations range from coastal plain to storm-influenced shelf conglomerates, while carbonate facies associations range from mid-shelf to slope (Saylor, 2003).

A sequence stratigraphic framework has been developed for the Kuibis and Schwarzrand Subgroups in the Witputs subbasin (Saylor, 2003; Saylor et al., 1995, 2005). The Kuibis Subgroup consists of two large-scale depositional sequences (K1-2) and the Schwarzrand Subgroup consists of six large-scale sequences (S1-6; Fig. 1b), several of which are bound by subaerial unconformities (Saylor, 2003; Saylor et al., 1995, 2005). Additionally, medium- and small-scale sequences have been recognized in the Huns, Feldschuhhorn and Spitskop Members (Saylor, 2003; Saylor et al., 2005). In total, eighteen medium-scale sequences were recognized in this succession (Saylor, 2003; Saylor et al., 2005). From small to large, the three scales of sequences have thicknesses of less than one to tens of meters, several tens of meters, and tens to hundreds of meters (Saylor, 2003). Based on the then available U-Pb zircon ages (Grotzinger et al., 1995), these were estimated to span a few tens of thousands of years, a few hundreds of thousands of years, and one to two million years, respectively (Saylor, 2003).

2.5. Geochemical proxies

The Nama Group has been the subject of multiple chemostratigraphic studies, which have included carbonate carbon and oxygen isotopes ($\delta^{13}C$ and $\delta^{18}O$; Kaufman et al., 1991; Nelson et al., 2022; Ries et al., 2009; Saylor et al., 1998; Wood et al., 2015), sulfur isotopes ($\delta^{34}S$; Ries et al., 2009; Tostevin et al., 2017), calcium isotopes ($\delta^{44}Ca$; Tostevin et al., 2019a), uranium isotopes ($\delta^{238}U$; Tostevin et al., 2019b), iron speciation (Bowyer et al., 2020; Darroch et al., 2015; Sperling et al., 2015; Wood et al., 2015), phosphorus speciation (Bowyer et al., 2020), total organic carbon (TOC; Bowyer et al., 2020; Darroch et al., 2015; Sperling et al., 2015; Wood et al., 2015), and cerium anomalies (Tostevin et al., 2016). However, the resolution is generally too coarse to permit direct comparison of chemostratigraphic variations with small- and medium-scale sequences or to perform cyclostratigraphic analysis.

The $\delta^{13}C$ of the Nama Group displays globally-recognized trends for the late Ediacaran, suggesting that the Nama Basin was connected to the open ocean (Kaufman et al., 1991; Saylor et al., 1998). The lower Kuibis Subgroup records a recovery from strongly negative $\delta^{13}C$ values, termed the basal Nama excursion (BANE; Bowyer et al., 2022), while values in the Urusis Formation remain relatively constant between ~0–3‰ (Ries et al., 2009; Saylor et al., 1998). The BANE might represent the end of the Shuram excursion (Wood et al., 2015) or another, younger perturbation (Bowyer et al., 2022). The large negative excursion marking the Ediacaran-Cambrian boundary, termed the basal Cambrian carbon isotope excursion (BACE), is not recognized in the Nama Group (Bowyer et al., 2022; Nelson et al., 2022).

Iron speciation data from the lower Nama Group indicate that the Zaris and Witputs subbasins were mostly anoxic and ferruginous in deep settings (outer ramp), while redox conditions in shallow settings (mid and inner ramp) were highly variable and episodically oxic (Bowyer et al., 2020; Wood et al., 2015). In the upper Nama Group, deep and shallow settings are generally interpreted to have been more oxygenated (Bowyer et al., 2020; Darroch et al., 2015; Wood et al., 2015).

Table 1
Published high-precision U-Pb zircon ages from volcanic ash beds in the Witputs subbasin.

Ash bed	Lithostratigraphic position	Age (Ma)	Latitude	Longitude
W8	Nomtsas Formation	538.58 +/- 0.19[1]	−27.444056	16.558722
W7	Upper Spitskop Member	538.99 +/- 0.21[1]	−27.474278	16.693306
W6	Upper Spitskop Member	539.64 +/- 0.19[1]	−27.474111	16.693194
W5	Upper Spitskop Member	539.52 +/- 0.14[1]	−27.474194	16.693000
W4	Upper Spitskop Member	539.58 +/- 0.34[1]	−27.474194	16.693000
W3	Upper Spitskop Member	540.095 +/- 0.099[1]	−27.473028	16.694417
W2	Lower Nasep Member	542.65 +/- 0.15[2]	−27.339690	16.698260
W1	Base Nudaus Formation	545.27 +/- 0.11[2]	−27.221520	16.792460

[1] Linnemann et al. (2019).
[2] Nelson et al. (2022).

2.6. U-Pb geochronology

Initial radiometric age control of the Nama Group was provided by U-Pb zircon dating using Isotope Dilution-Thermal Ionization Mass Spectrometry (ID-TIMS) of four volcanic ash beds: one from the Kuibis Subgroup in the Zaris subbasin, two from the Spitskop Member in the Witputs subbasin, and one from the Nomtsas Formation in the Witputs subbasin (Grotzinger et al., 1995). However, these ages had relatively large uncertainties of ~1 m.y. compared with the precision that can be achieved with modern ID-TIMS techniques.

More recently, zircons from fifteen volcanic ash beds in the Nama Group were dated using chemical Abrasion-Isotope Dilution-Thermal Ionization Mass Spectrometry (CA-ID-TIMS) techniques, yielding U-Pb ages with small analytical uncertainties of 0.1–0.3 m.y. One ash bed is located in the Kuibis Subgroup in the Zaris subbasin (Bowring et al., 2007), six are located in the middle to upper Schwarzrand Subgroup in the Vioolsdrift area (Nelson et al., 2022), and eight are located in the Witputs subbasin (Fig. 1b).

In the Witputs subbasin, two are positioned in the lower part of the Schwarzrand Subgroup: one at the base of the Nudaus Formation (W1) and one in the lower Nasep Member (W2; Nelson et al., 2022). The other six are positioned in the upper Schwarzrand Subgroup: five in the upper Spitskop Member (W3-7) and one in the Nomtsas Formation (W8; Linnemann et al., 2019). These ash beds yield ages between ~545 and ~539 Ma (Table 1).

3. Methods

The Nudaus and Urusis Formations of the Nama Group in the Witputs subbasin were analyzed with Google Earth satellite images. These formations are extensively exposed in the area between latitudes of −27.1 and −28.0 and longitudes of 16.1 and 17.5 (e.g., Fig. 1 of Bowyer et al., 2020). The Kuibis Subgroup is excluded at this stage because there are no volcanic ash beds dated for this succession in the Witputs subbasin that can be used for independent testing of cyclostratigraphic interpretations.

By using published geological maps and lithological descriptions, the lithological units could be confidently recognized on the satellite images. Sedimentary alternations are recognized based on differences in color, relief, and texture. Here, a sedimentary alternation is defined as a recessive lower section followed by a resistant upper section. The resistant beds of alternations on the dominant scale were labelled in each selected location. Clear alternations were indicted with numbers and uncertain alternations were indicated with letters. This was done for each lithostratigraphic unit, from bottom to top in increasing and alphabetical order.

Thicknesses were estimated using Google Earth elevation data without correcting for the dip of the bedding. Sediment color descriptions were based on satellite images and could be influenced by the hue of the image. The entire area was thoroughly scanned to determine lateral variations and consistent patterns. Sections were selected that contain the most complete stratigraphy and clearest sedimentary alternations, preferably with minimal deformation. This information was used to develop an initial cyclostratigraphic framework.

The dated volcanic ash beds were correlated to the cyclostratigraphic framework using their coordinates and logged stratigraphic positions. Subsequently, their high-precision U-Pb zircon ages (Linnemann et al., 2019; Nelson et al., 2022) were used to determine the average duration of alternations.

4. Results

Several locations were studied, which are distributed throughout the Witputs subbasin (Fig. 2). Here, we show the outcrops with the most complete stratigraphy and clearest sedimentary alternations. The labelled satellite images and coordinates of the other outcrops are included in the supplementary material (Figs. S1-22; Table S1).

4.1. Dominant (medium-scale) alternations

4.1.1. Nudaus Formation

Outcrops of the Nudaus Formation consist of recessive green–blue gray colored shales interspersed with coarser, more resistant sandstone beds (Saylor et al., 1995; Fig. 3). The labelled, resistant parts typically consist of two to three closely spaced beds. At least thirteen resistant parts (i.e., fourteen alternations) are recognized within the Nudaus Formation. The base is referred to as Nu0. The lower beds related to Nu1-3 are less resistant than the overlying beds related to Nu4-8. Above Nu8, there is a relatively thick, recessive interval, overlain by the relatively resistant beds related to Nu9-13.

Three additional resistant parts might be present (Nu0a, Nu10a, Nu13a), totaling up to sixteen resistant parts in the Nudaus Formation. The recognition of Nu0a below Nu1 is restricted to only a small geographic area (at location 2). Nu10 and Nu10a occur closer together than other resistant parts, making it difficult to establish if they represent one or two alternations. At location 1, the interval between Nu13 and the base of the Nasep Member (bed Na1) is thicker than at other locations and at least one extra alternation (Nu13a) can be recognized (Fig. 3). Here, smaller-scale variations are also visible. The upper part of this section might have been eroded at the other locations. Lastly, the relatively thick interval between Nu8 and Nu9 might represent more than one alternation, increasing the maximum number of resistant parts in the Nudaus Formation to more than sixteen. Where alternations are well recognizable, mostly on the western side of the study area, they are on average ~17–22 m thick.

4.1.2. Nasep Member

Outcrops of the Nasep Member generally consist of green–blue gray shales (similar to the Nudaus Formation) and thick-bedded, coarse, reddish sandstone (Saylor et al., 1995; Figs. 4 and 5). The Nasep Member often initiates and terminates with distinct red sandstone units (Na1 and Na8; Saylor et al., 1995). However, the Nasep Member shows significant lateral variation: green–blue gray shales are more common to the west, while red sandstones are more common towards the east (Saylor et al.,

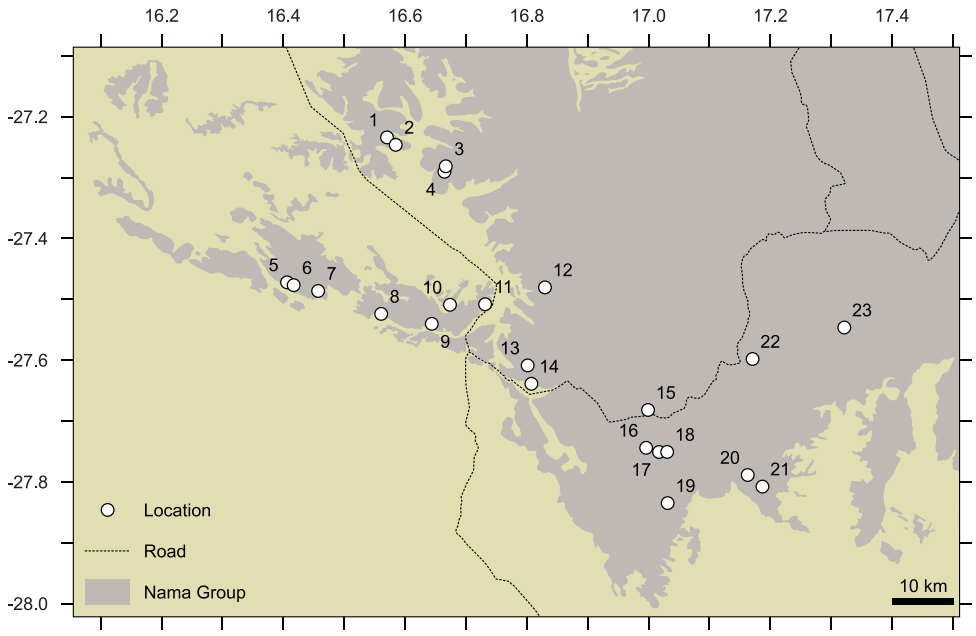

Fig. 2. Map of the study area showing outcrop areas of the Nama Group and studied locations.

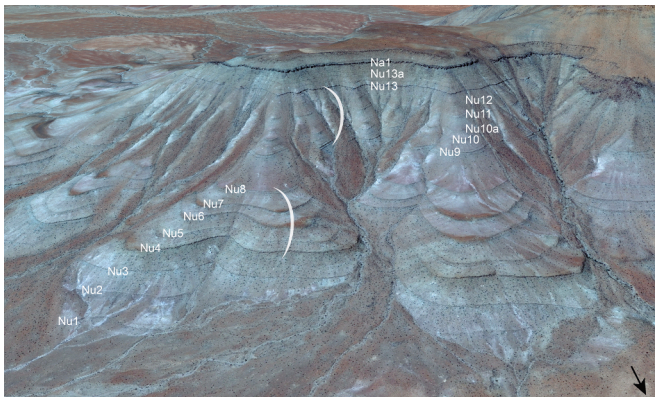

Fig. 3. Satellite image with labelled alternations of the Nudaus Formation at location 1 (latitude −27.234003, longitude 16.570064). Large-scale variations are indicated by the arches. The black arrow on the bottom right indicates the north direction. Image: Google Earth, © 2023 Maxar Technologies (accessed 15 May 2023).

Fig. 4. Satellite image with labelled alternations of the Nasep Member at location 13 (latitude −27.608656, longitude 16.801131). The black arrow on the bottom right indicates the north direction. Image: Google Earth, © 2023 Maxar Technologies (accessed 15 May 2023).

1995). Furthermore, western exposures are typically covered by red sandstone debris derived from the uppermost part (Na8), making the identification of alternations difficult. (North)western exposures (i.e., locations 1, 3, 5–9, and 13–14) are thickest (~100–200 m) and encompass a maximum of eight resistant parts (Fig. 4), while (south) eastern exposures (i.e., locations 18–21 and 23) are significantly thinner (~30–110 m) with usually only three recognizable resistant parts. Additionally, western exposures are thickest towards the south (~180 m at locations 13 and 14) compared to the northwest (~100 m at locations 1 and 3). In the northwest, the dark gray colored bed Na2, likely representing a calcarenite limestone unit (Saylor et al., 1995), is positioned closer to Na1 compared to towards the south. Alternations are on average ~28 m thick in western exposures (locations 13 and 5–7).

In the west, Na4 usually has a red color and forms a small plateau, which likely correlates to the middle alternation in the east. Alternatively, the middle alternation in the east could correlate with Na2. This implies that only Na1, Na4 or Na2, and Na8 are present in eastern exposures. The thinner succession and absence of alternations below Na8 in the east suggests that erosion likely occurred below Na8.

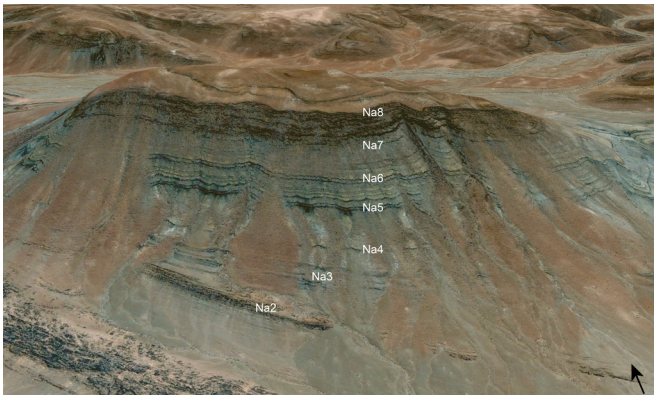

Fig. 5. Satellite image with labelled alternations of the Nasep Member at location 5 (latitude −27.472136, longitude 16.405878). The black arrow on the bottom right indicates the north direction. Image: Google Earth, © 2023 Maxar Technologies (accessed 15 May 2023).

4.1.3. Huns, Feldschuhhorn, and lower Spitskop Members

Outcrops of the Huns, Feldschuhhorn and lower Spitskop Members are very similar in appearance and therefore are combined into a single section for the purpose of our analysis. The contact between the lower and middle Spitskop Members is easily recognized due to a significant change in the weathering profile. However, the Feldschuhhorn Member is not recognized and therefore the entire section is labelled with similar codification (i.e., starting with 'H').

The succession consists of regular alternations between gray to blue gray recessive shales and dark gray to bluish resistant carbonate beds (Saylor et al., 1995; Fig. 6). A minimum of ten resistant parts are recognized in this succession. H1 typically separates underlying reddish from overlying blue to gray sediments. Thus, the first alternation is still similar in appearance to the Nasep Member, consisting of a transitional, mixed siliciclastic-carbonate interval (Saylor et al., 1995). H4 is a distinct resistant interval that consists of many smaller-scale variations. Alternations H8-10 are slightly thinner than the underlying alternations.

An additional alternation, H9a, might be present between H9 and H10, increasing the total number of resistant parts in the succession to eleven. In the Huns Mountains (e.g., at location 22), it is not clear if the uppermost alternation correlates to H9a or H10. At location 17, H10 seems to consist of two beds closely spaced together and the lower one might represent H9a. The average thickness of an alternation varies between ~18 and ~48 m throughout the study area. Alternations are thickest on the southwest side of the Huns Mountains (locations 20 and 21).

4.1.4. Middle and upper Spitskop Member

Outcrops of the middle and upper part of the Spitskop Member consist of alternations of green–blue gray to red recessive shales topped by dark gray carbonate beds (Saylor et al., 1995; Fig. 7). At least five alternations are present in this succession, which are thicker than those in the section below it. This suggests that either the sedimentation rate increased or that the thicker alternations reflect larger-scale alternations. The first alternation begins with a distinct dark gray bed that often appears as a wavy outline in the surrounding lighter-colored sediments. The second alternation usually contains relatively pronounced smaller-scale variations. Just below the resistant part S4, a distinct lighter and bluer interval is present. The alternations are ~38 m thick at location 16 and ~38–69 m at locations 10 and 11.

4.2. Large- and small-scale variations

Besides the alternations on the dominant scale, smaller- and larger-scale variations are recognized. Although the Kuibis Subgroup has not been analyzed here, it is important to note that it shows particularly clear large-scale bundling patterns (Fig. 8). In the Nudaus Formation, two bundles of relatively resistant parts occur (Nu4-8 and Nu9-13), each spanning four to five dominant alternations (Fig. 3). The Nasep Member begins and ends with a thick sandstone unit (Fig. 4), possibly representing one large-scale alternation. However, as the reddish Na4 is often relatively resistant, the Nasep Member might also consist of two large-scale alternations. At south Arimas, Na8, H3, H6-7 and H10 are slightly thicker and more resistant than the resistant parts in between (Fig. 6). These pronounced resistant parts occur regularly, separated by three to four alternations on the dominant scale. S3 is also relatively thick and resistant, separated from the underlying H10 by three dominant alternations (Fig. 7). These observation around location 17 imply a ratio between large- and dominant-scale alternations of 1:3 to 1:4.

In some cases, beds occur on a smaller scale than the dominant alternations. In the Nudaus Formation, two to three beds typically occur closely spaced together, forming one resistant part on the dominant scale (Fig. 3). In the area towards the west (locations 5–8), pronounced small-scale variations are present between Na5 and Na8 (Fig. 5 and S14). Seven small-scale alternations are present between Na5 and Na6, and five, or possibly six, occur between Na6 and Na7. Small-scale alternations are difficult to count between Na7 and Na8. In the Huns Member around locations 15 and 17, six small-scale alternations occur between H4 and H5 (Fig. S14). This means that a maximum of five to seven small-scale alternations can be recognized per dominant alternation.

5. Integration of stratigraphic data

5.1. Integration of U-Pb ages

The positions of dated volcanic ash beds are correlated to our cyclostratigraphic framework (Fig. 9). The oldest age constraint in the Witputs subbasin is provided by a volcanic ash bed at the base of the Nudaus Formation (Table 1; Nelson et al., 2022), for which we assume a lowermost position of Nu0. At this location, however, the lowest part of the Nudaus Formation is not present (Fig. S24), meaning that this ash bed could also be positioned slightly higher in the stratigraphy (up to Nu2). The dated ash bed in the lower Nasep Member is located just above a limestone bed (Nelson et al., 2022), which is correlated to bed Na2 (Fig. S25). Five dated ash beds are positioned in a limestone unit in the upper Spitskop Member (Linnemann et al., 2019) that correlates to bed S4 (Fig. S26).

Average durations of alternations are calculated for three different cyclostratigraphic intervals: from the base of the Nudaus Formation to the upper Spitskop Member (Nu0-S4), from the base of the Nudaus

Fig. 6. Satellite image with labelled alternations of the Huns, Feldschuhhorn and lower Spitskop Members at location 17 (latitude −27.750900, longitude 17.016972). Large-scale variations are indicated by the arches. The black arrow on the bottom right indicates the north direction. Image: Google Earth, © 2023 CNES / Airbus (accessed 15 May 2023).

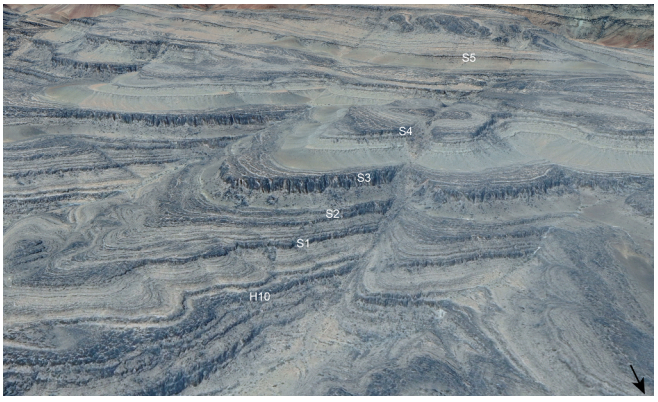

Fig. 7. Satellite image with labelled alternations of the middle to upper Spitskop Member at location 16 (latitude −27.744078, longitude 16.995842). The black arrow on the bottom right indicates the north direction. Image: Google Earth, © 2023 CNES / Airbus (accessed 15 May 2023).

Fig. 8. Satellite image of the Kuibis Subgroup in the Zaris subbasin (latitude −24.593050, longitude 16.177456). Alternations and bundling patterns are indicated by the arches. The black arrow on the bottom right indicates the north direction. Image: Google Earth, © 2023 Maxar Technologies (accessed 15 May 2023).

Formation to the lower Nasep Member (Nu0-Na2), and from the lower Nasep Member to the upper Spitskop Member (Na2-S4; Table 2). However, the age difference between the lower (W3) and upper (W7) ash beds that are positioned around bed S4 is significant, namely 1.105 +/- 0.309 m.y. (Table 1). Both W3 and W7 are used for calculating durations, providing a lower and upper estimate, respectively. For each cyclostratigraphic interval, the uncertainty in the number of alternations is considered (i.e., excluding and including uncertain alternations). This results in average durations of ~120–180 k.y. (Table 2).

5.2. Comparison with sequence stratigraphy

5.2.1. Medium and small scale

The dominant alternations identified on the satellite images are comparable in thickness to the medium-scale sequences in the sequence stratigraphic framework of Saylor (2003) and Saylor et al. (2005). However, there is a discrepancy between the number of dominant alternations and medium-scale sequences, which originates from different conceptions of scale. Fifteen alternations versus eighteen medium-scale sequences are recognized in the Huns to Spitskop Members (Saylor, 2003; Saylor et al., 2005). In some cases, two successive medium-scale sequences (namely 2–3, 6–7 and 13–14) are approximately half the thickness of the surrounding sequences (Fig. 4c of Saylor, 2003; Fig. 4a of Saylor et al., 2005). Merging these successive, thinner medium-scale sequences into one alternation solves the observed discrepancy (Fig. 9). Both the sandier-upward cycles in the Nudaus Formation and the medium-scale sequences in the Huns to Spitskop Members, often consisting of a siliciclastic-rich lower or middle part and a carbonate-rich top, were interpreted as shallowing-upward cycles (Saylor et al., 1995; Saylor, 2003). Thus, our labelled resistant beds correspond to the tops of these shallowing-upward cycles.

Twenty-five small-scale sequences were recognized in medium-scale sequences 4–9 (Saylor, 2003), corresponding to our alternations H3-7. This results in an average of five small-scale alternations per dominant alternation and roughly corresponds to our estimate of maximum five to seven small-scale alternations per dominant alternation.

The Feldschuhhorn Member is placed in the lower part of medium-scale sequence 10 of Saylor et al. (2005), which corresponds to the lower part of our alternation H8 (Fig. 9). The overlying alternations H9-10 are part of the lower Spitskop Member. However, in our studied sections at least, the recessive interval of alternation H8 is

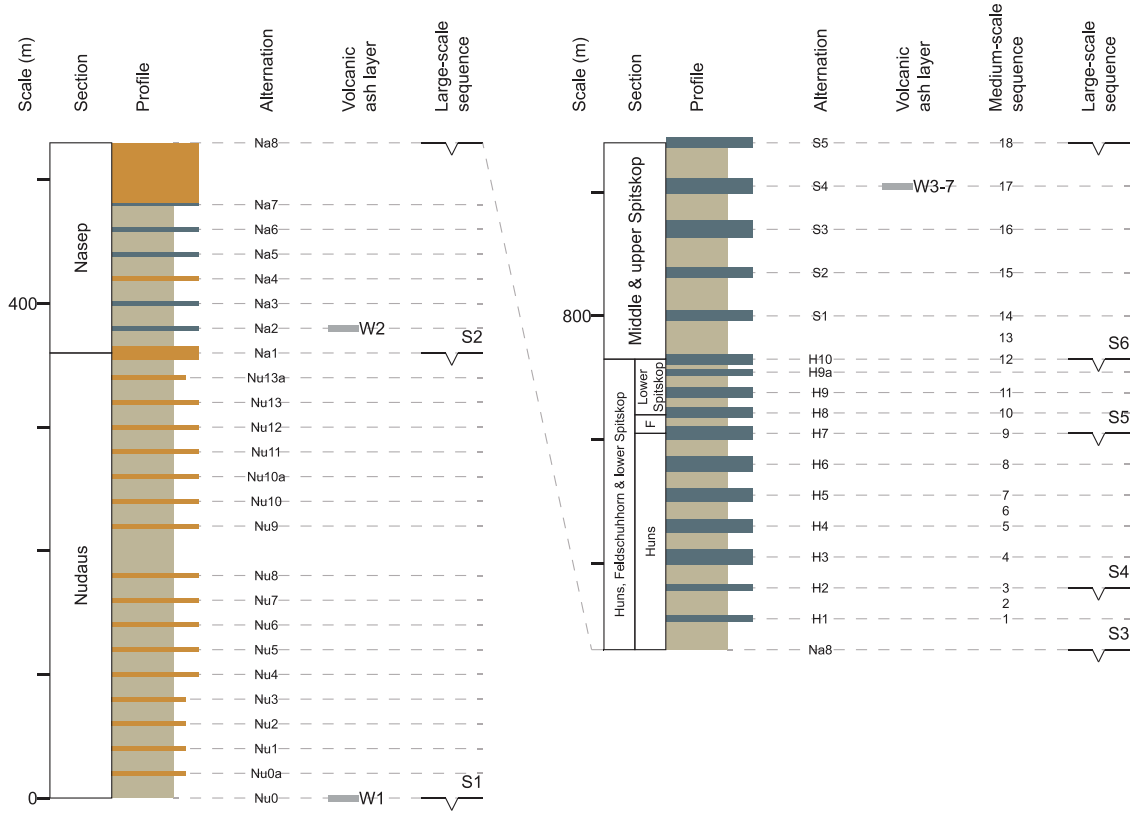

Fig. 9. Schematic overview of the initial cyclostratigraphic framework based on locations 1, 13–14, and 16–17 and the comparison with the published high-precision U-Pb ages (Nelson et al., 2022; Linnemann et al., 2019) and sequence stratigraphic framework (Saylor, 2003; Saylor et al., 2005). F = Feldschuhhorn.

Table 2
Calculation of average durations of alternations.

Ash beds	Cyclostratigraphic interval	Duration (m.y.)	Number of alternations	Average duration of alternations (k.y)
W2-W7	Na2-S4$_{upper}$	3.66 +/- 0.36	20	183 +/- 18
			21	174 +/- 17
W2-W3	Na2-S4$_{lower}$	2.555 +/- 0.249	20	128 +/- 12
			21	122 +/- 12
W1-W2	Nu0-Na2	2.62 +/- 0.26	15	175 +/- 17
			18	146 +/- 14
W1-W7	Nu0-S4$_{upper}$	6.28 +/- 0.32	35	179 +/- 9
			39	161 +/- 8
W1-W3	Nu0-S4$_{lower}$	5.175 +/- 0.209	35	148 +/- 6
			39	133 +/- 5

indistinguishable from those in the underlying or overlying alternations. Therefore, it is not feasible to place this interval in a separate lithostratigraphic unit.

5.2.2. Large scale

The large-scale variations recognized on satellite images (based on differences in the expression of medium-scale alternations) differ from the identified large-scale sequences (Fig. 9). Although two bundles were recognized in the Nudaus Formation, these only correspond to one large-scale sequence (namely S1; Saylor et al., 1995). Three large-scale sequences are observed in the Huns to lower Spitskop Member (S3-5; Saylor, 2003), which differ slightly in terms of placement from the observed large-scale variations. The basal sequence boundaries of S4 and S5 are located slightly lower and higher, respectively, than the boundaries of our large-scale variations. Therefore, S4 consists of more medium-scale sequences than S3 and S5, while we observed a more or less constant ratio between large- and medium-scale alternations in this interval as expected in the case of astronomical forcing.

5.2.3. Lateral variations

The Nasep Member shows significant lateral variation and therefore its alternations are difficult to correlate throughout the area. Saylor et al. (1995) noted that the middle shale interval thins eastward, which is also observed on the satellite images. Although this could be an indication for erosion beneath the top sandstone unit (Na8), no evidence for this was found in the field (Saylor et al., 1995). Instead, it was proposed to originate simply from delta progradation (Saylor et al., 1995). However, this might not explain the lower number of alternations recognized in eastern sections.

A sequence boundary was placed above the sandstone unit (Na8) because of an erosional surface that cuts through most of the Nasep Member towards the northeast of the Huns Mountains (landward margin; Saylor et al., 1995). This is outside of our studied area and therefore agrees with the continuous presence of this bed in our studied sections.

In the sequence stratigraphic framework of Saylor (2003), medium-scale sequences 1 and 2 of the lower Huns Member disappear towards the east, starting from Abos (to the west of the Huns Mountains). However, these sequences correspond to alternations H1 and H2 (Fig. 9), which can still be recognized in this area as well as on the east side of the Huns Mountains (location 23).

6. Discussion

6.1. Cyclostratigraphic interpretations

The regularity of the sedimentary variations in the Nama Group, which are continuous throughout the Witputs subbasin, is suggestive of an astronomical origin. Based on the existing U-Pb ages, the alternations have a duration of ~120–180 k.y. (Table 2), which falls within the frequency band of astronomical forcing. We consider two possible astronomical interpretations in which the dominant alternations are related to (1) ~100 k.y. short eccentricity or (2) 173 k.y. obliquity amplitude modulation. Both cycles have periods that fall within or are close to the estimated U-Pb-based cycle durations.

6.1.1. Short eccentricity

If the dominant alternations are related to short eccentricity, then the smaller and larger variations are expected to be related to precession and long eccentricity as eccentricity modulates the amplitude of precession. Even though the Solar System behaves chaotically, the periods of the long (405 k.y.) and short (~100 k.y.) eccentricity cycles, and therefore their ratio of approximately 1:4, remained relatively stable over at least the last 250 m.y. (Laskar et al., 2011). The periods of precession (~22 k.y.) and obliquity (~41 k.y.), in contrast, decreased back in time due to the evolution of the Earth-Moon system (Laskar et al., 2011). Cyclostratigraphic estimates indicate ~18 k.y. precession and ~30 k.y. obliquity periods for the Cambrian (Fang et al., 2020; Sørensen et al., 2020; Zhang, Li, et al., 2022) and a further decrease to ~14 k.y. precession at ~1.4 Ga (Meyers and Malinverno, 2018) and ~11 k.y. precession at ~2.5 Ga (Lantink et al., 2022). These estimates roughly agree with most ocean models for lunar regression (Fig. 5 of Lantink et al., 2022; Daher et al., 2021; Waltham, 2015; Webb, 1982) and fit exceptionally well with the recently presented combined global and hemispherical ocean model (Farhat et al., 2022). This implies that the ratio between short eccentricity (~100 k.y.) and precession changed from 1:~4.5 to 1:~5.6. These ratios roughly agree with the observed ratio between large and dominant-scale alternations around location 17 (namely 1:3 to 1:4) and the presence of five to seven small-scale alternations within one dominant-scale alternation.

The average period of short eccentricity is relatively close to, but slightly lower than, the estimated cycle durations. As the Nama Group was mostly deposited in shallow marine environments and contains several major sequence boundaries, the presence of hiatuses is expected. If alternations are missing, the total number of alternations increases and therefore the inferred cycle duration decreases, bringing it closer to ~100 k.y. In addition, missing dominant alternations could disturb large-scale patterns related to long eccentricity. The relatively large cycle duration for the Nu0-Na2 interval might be (partly) related to the regional erosional unconformity associated with the sequence boundary that separates the Nudaus Formation from the Nasep Member (Saylor et al., 1995; Saylor, 2003). Three sequence boundaries are present within the Na2-S4 interval and might contain missing alternations. As some alternations are missing in eastern exposures of the Nasep Member, it might be possible that western exposures are also not complete.

The dominant alternations of the middle to upper Spitskop Member are thicker compared to those in the underlying successions. If they were related to 405 k.y. long eccentricity, this would reduce the cycle duration of the underlying alternations that are related to short eccentricity (Table S4). However, especially around location 17, where an entire Huns to upper Spitskop succession is present, the differences in thickness do not seem significant enough for this scenario and it seems more likely that the labelled alternations all represent the same timescale.

6.1.2. Obliquity amplitude modulation

Alternatively, the dominant alternations could be related to the 173 k.y. amplitude modulation cycle of obliquity. A dominant control by this modulation cycle would be remarkable, although Huang et al. (2021) suggest that this cycle might be more often expressed as generally assumed. It has been proposed that Precambrian obliquity was much higher than today (>54°) in order to explain the low-latitude glaciations of the Cryogenian (Williams, 1993), which would have significantly increased the seasonality. However, it has been shown that Earth's obliquity is stabilized by the presence of the Moon (Laskar et al., 1993) and the mechanism proposed for the required rapid decrease in obliquity (~30° between 650 and 430 Ma; Williams et al., 1998) has been invalidated (Levrard and Laskar, 2003). Moreover, the combined model even shows a decrease in obliquity back in time (Fig. 6 of Farhat et al., 2022).

In the case of dominant 173 k.y. cycles, the smaller and larger variations could be related to obliquity and ~1.2 m.y. obliquity modulation. Both the 173 k.y. and ~1.2 m.y. cycles are unaffected by the Earth-Moon system. The 173 k.y. cycle probably remained relatively stable (Boulila et al., 2018; Charbonnier et al., 2018), while the period of the ~1.2 m.y. cycle (and therefore their ratio of 1:7) might be affected by chaotic behavior related to the Mars-Earth secular resonance (Laskar et al., 2011; Olsen et al., 2019). In many astronomical solutions, this period remained between 1.0 and 1.4 m.y. over the last 250 m.y. (Fig. 7a of Olsen et al., 2019), meaning that the ratio with the 173 k.y. cycle varied between 1:6 and 1:8. This differs significantly from the observed 1:3 to 1:4 ratio around location 17 and slightly from the bundles in the Nudaus Formation consisting of four to five dominant alternations. The ratios between 173 k.y. and ~ 30 k.y. obliquity (1:5.8) and between ~100 k.y. eccentricity and ~18 k.y. precession (1:5.6) are similar and therefore both options fit the observations.

The period of 173 k.y. is very close to the maximum estimated cycle durations based on U-Pb ages (Table 2), meaning that no cycles would be missing even though deposition occurred in mostly shallow marine environments. However, time could still be missing if parts of the cycles are not preserved. If all cycles are preserved, the large-scale patterns cannot be disturbed due to missing dominant alternations. Therefore, unlike in the case of short eccentricity, missing alternations cannot explain the inconsistencies between expected and observed large-scale patterns. This alternative interpretation is only consistent with the minimum number of alternations in the Nudaus Formation and the older age of ash bed W7 for S4, as all other estimated cycle durations are significantly lower than 173 k.y.

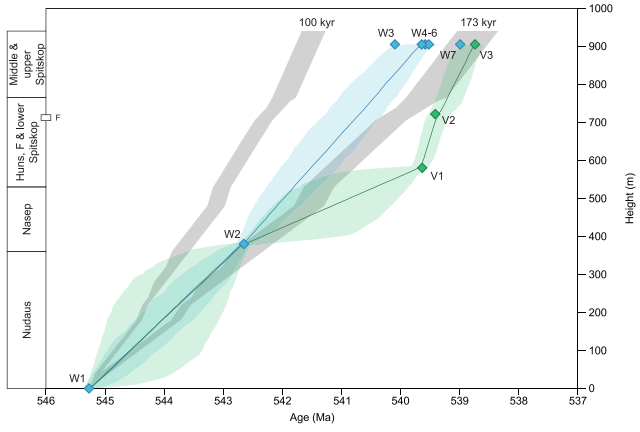

Fig. 10. Comparison of age models based on high-precision U-Pb ages from the Witputs subbasin (blue) and Vioolsdrift area (green) and the cyclostratigraphic interpretations (grey). Bayesian age models were created with Bchron (Haslett and Parnell, 2008) and plotted with their median (blue/green solid line) and 95% confidence interval (blue/green shaded area). Positions of the U-Pb ages are indicated by the blue/green diamonds. All data is plotted on the stratigraphy presented in Fig. 9. The Vioolsdrift U-Pb ages were transferred to the Witputs stratigraphy based on lithostratigraphic correlations (Nelson et al., 2022). The cyclostratigraphic interpretations include a minimum and maximum number of alternations (Table 2). F = Feldschuhhorn. (For interpretation of the references to color in this figure legend, the reader is referred to the web version of this article.)

6.2. Uncertainties of U-Pb ages

Comparison of the high-precision U-Pb ages within the Witputs subbasin as well as with the ones from the Vioolsdrift area reveals significant differences in their age-depth distribution (Fig. 10). Volcanic ash beds W3-7 are all present within alternation S4 and are therefore expected to have relatively similar ages (differing not more than the cycle length). However, W3 and W7 differ in age by ~1.1 +/- 0.3 m.y., while W4-6 all have relatively similar ages that fall approximately in the middle of this age range (Table 1). Compared to the U-Pb ages from the Witputs subbasin, the ones from the Vioolsdrift area are much younger than expected based on their lithostratigraphic position. The ages from the lower Huns Member (V1) and the base of the Spitskop Member (V2) differ in age by only ~0.22 +/- 0.6 m.y. and are both similar in age to W4-6 from the upper Spitskop Member. This might suggest that the lithostratigraphy-based correlations between the areas (Fig. 9 of Nelson et al., 2022) are not isochronous. An attempt to correlate the areas based on cyclostratigraphy suggests that V1 is positioned slightly higher up in the lithostratigraphy (H6 in the upper Huns Member; Figs. S22 and S27). However, this does not entirely solve the observed discrepancies.

Based on the combination of W1-2 and V1-3, it was suggested that a significant change in sedimentation rate occurred during deposition of the Nama Group (Nelson et al., 2022). In contrast, our cyclostratigraphic framework indicates a relatively stable sedimentation rate. The cyclostratigraphic model based on 173 k.y. per alternation is consistent with W2 (only when assuming a minimum number of alternations) and W7 and V3, however, implies that V1-2 and W3-6 are incorrect. The model based on 100 k.y. per alternation results in a higher sedimentation rate, which is relatively similar to that indicated by V1-3, but requires hiatuses to be in agreement with the U-Pb ages. These hiatuses might be present at the sequence boundaries at top of the Nudaus Member and the top of the Nasep Member, or, alternatively, below the top sandstone unit of the Nasep Member as suggested by our cyclostratigraphic framework. Therefore, rather than a significant change in sedimentation rate, our results suggest the presence of hiatuses within the Nama Group.

6.3. Origin of the sequences

Previously, both tectonism and eustasy have been proposed to explain the different scales of sequences in the Urusis Formation (Saylor, 2003). Some large-scale sequences (S3, S5, and S6) show asymmetric patterns typical of flexural bending of the basin (Catuneanu et al., 1997), while others (S2, S4, and top S6) might instead be eustatically controlled (Saylor, 2003). This suggests that both tectonics and astronomical climate forcing affected the sedimentation on these longer timescales, which might have caused differences in the recognition of large-scale variations between the cyclo- and sequence stratigraphic frameworks. Additionally, interference of tectonic processes could complicate the recording of regular large-scale variations related to astronomical forcing.

On the medium and small scale, the occurrence of siliciclastic deposits in the middle of the sequences might be explained by glacio-eustasy or flexural bending (Saylor, 2003). It was estimated that internal tectonic variability, although related to thrust deformation, can occur on timescales of 0.15–4 m.y. (Naylor and Sinclair, 2007), of which the lowermost value is similar to the estimated duration of medium-scale sequences. However, it is much larger than the duration of smaller-scale variations (~120–180 k.y. divided by 5–7). Therefore, the regularity, high-frequency, and hierarchical stacking of these sedimentary variations are not easily explained by tectonic processes, while they

are indicative of astronomical climate forcing. The correlatability over a large geographic area also seems to exclude an autogenic origin of the sequences.

In principle, instead of being of eustatic origin, the sequences could also be related to variable terrigenous influx rates from the hinterland associated with astronomical-induced changes in monsoon intensity. This low-latitude mechanism, typically driven by precession and eccentricity, has been used to explain shallow marine sequences in the Cretaceous greenhouse when glacio-eustasy is thought to be minor or absent (e.g., García et al., 1996). However, this cannot (easily) explain the observed shallowing-upward sequences that are marked at the top by exposure surfaces like karst or desiccation cracks (Saylor, 2003).

Astronomically-forced fluctuations in eustatic sea level could occur through water storage in groundwater (aquifer-eustasy) or ice sheets (glacio-eustasy). Aquifer-eustasy was proposed for sea-level fluctuations during greenhouse periods of the Cretaceous and early Cambrian, which were mainly paced by the long (~1.2 m.y.) obliquity amplitude modulation cycle (Wendler et al., 2016; Zhang, Li, et al., 2022; Zhang, Huang, et al., 2022). Obliquity controls the seasonal contrast and therefore poleward moisture and heat transport, which in turn affects aquifer storage in middle to high latitudes (Wendler and Wendler, 2016). The ~173 k.y. obliquity amplitude modulation cycle affected the carbon cycle in middle to high latitudes during parts of the Mesozoic and Cenozoic, probably through hydrological processes (Huang et al., 2021), suggesting it could also drive aquifer-eustasy. However, simulations indicate that aquifer-eustasy cannot account for significant sea-level fluctuations (Davies et al., 2020).

Glacio-eustasy might be a more probable cause for the sea-level fluctuations recorded in the Nama Basin, as there is some evidence for glaciation throughout the late Ediacaran (e.g., Chen et al., 2020; Chumakov, 2011; Germs and Gaucher, 2012; Linnemann et al., 2022; Wang et al., 2023). During the Pliocene and early Pleistocene, glaciations were dominantly paced by 41 k.y. obliquity (Lisiecki and Raymo, 2005) and throughout the Cenozoic third-order glacio-eustatic sequences were mainly controlled by the ~ 1.2 m.y. obliquity modulation cycle (Boulila et al., 2011). Although spectral power is present around ~ 173 k.y. in the $\delta^{18}O$ inferred sea-level curve for the interval ~ 1–9 Ma, it is much lower compared to power at ~ 1.2 m.y. and 41 k.y. (Boulila et al., 2011; Miller et al., 2005). Therefore, it remains unclear if the ~ 173 k.y. obliquity cycle could have been responsible for the pronounced medium-scale sequences in the Nama Basin.

On the other hand, glaciations were strongly paced by ~ 100 k.y. eccentricity during the late Pleistocene (Imbrie and Imbrie, 1980; Lisiecki and Raymo, 2005) as well as throughout the Oligocene and Miocene along with ~ 400 k.y. eccentricity (Liebrand et al., 2016). Similar to the Nama Basin, regular sedimentary alternations and bundling patterns occur in the Donets Basin during the Carboniferous icehouse, ascribed to glacio-eustasy, which have been linked to ~ 100 and ~ 400 k.y. eccentricity based on U-Pb ages (Davydov et al., 2010). As ~ 100 k.y. eccentricity-paced glaciations and sea level changes are common throughout Earth's history, we suggest that the medium-scale sequences of the Nama Group are most likely related to ~ 100 k.y. eccentricity-paced glacio-eustasy, although a 173 k.y. obliquity pacing cannot be excluded.

6.4. Link between biota, redox conditions and sea level

6.4.1. Biotic distribution and oxygen

Changes in oceanic redox conditions have been linked to rises and falls of Ediacara biota (e.g., Evans et al., 2022; Wood and Erwin, 2018; Zhang et al., 2019), suggesting an important role of oxygen in the evolution of early complex life. Intervals of anoxia possibly resulted in extinction events (Evans et al., 2022), but also may have promoted evolutionary innovations (Wood and Erwin, 2018). Some Ediacara biota, however, were apparently able to tolerate low oxygen environments (Cherry et al., 2022).

Within the Nama Group, there is evidence for dynamic redox changes that may have acted as a primary control on fossil distributions (Tostevin et al., 2016; Wood et al., 2015). Metazoans often occur in oxic horizons with the most diverse communities in persistently oxygenated settings, while macroscopic animals were likely absent from anoxic, outer ramp environments (Tostevin et al., 2016; Wood et al., 2015). Although there seems to be a relationship between fossil distribution and redox state, the drivers behind these redox changes are not yet fully understood.

6.4.2. Mechanisms behind redox changes

Proposed mechanisms for anoxic phases in inner and mid ramp settings include high productivity and upwelling of anoxic deeper water (Bowyer et al., 2020; Wood et al., 2015). In the Kuibis Subgroup, relatively high TOC content of up to ~6 wt% occurs in an inner and outer ramp location of the Zaris subbasin (Zwartmodder and Brak; Wood et al., 2015), suggesting that productivity might have been high. This could have been related to a high influx of nutrients from the Kalahari Craton as indicated by high values of the chemical index of alteration (CIA; Bowyer et al., 2020). It was suggested that increased productivity led to anoxia (Bowyer et al., 2020) due to increased oxygen consumption via degradation of sinking organic matter. However, under low atmospheric oxygen levels, increased primary productivity could also result in oxygenated conditions in the photic zone (Lantink et al., 2023; Wei et al., 2021; Zhang, Li, et al., 2022). No systematic relationship has yet been found between (terrestrial) nutrient input, productivity, and redox state.

Instead, a correlation is observed between redox state and sequence stratigraphy (Wood et al., 2015), suggesting that (mechanisms behind) sea-level fluctuations controlled redox dynamics. In inner ramp settings, anoxic and ferruginous conditions often coincided with flooding events of m-scale shallowing-upward cycles in the Kuibis and Schwarzrand Subgroups (Wood et al., 2015). In contrast, reefs growing in mid ramp settings during transgressive systems tracts (TSTs) show persistent oxygenation, which is suggested to be due to a physical ventilation mechanism (Wood et al., 2015). However, the reefs might also have grown at water depths slightly shallower than inner ramp settings where conditions remained oxic as depicted by Tostevin et al. (2016). Moreover, variable redox conditions did occur in other mid-ramp locations (Bowyer et al., 2020). However, the two most diverse and complex trace fossil assemblages in the Witputs subbasin are found in the Nasep-Huns transition and the base of the Spitskop Member, both of which are preserved in transgressive settings between fair-weather and storm wave base (i.e., mid ramp; Darroch et al., 2021). Although this might be an indication of persistent oxygenation during TSTs, this is not (yet) confirmed by independent evidence from redox proxies.

Several different mechanisms could account for the development of anoxia during flooding or transgression. For the early Cambrian greenhouse, aquifer-eustatic transgression coincided with a mass extinction of small shelly fossils and was linked to flooding of the shelf with anoxic deep water (Zhang, Li, et al., 2022), while sea level lowering coincided with speciation events possibly due to the oxygenation of shallow waters (Zhuravlev et al., 2023). Possibly, the chemocline remained at a constant water depth, thereby changing its position relative to the margin with sea-level changes. For the late Ordovician to early Silurian icehouse, black shales and anoxia occurred during transgressions while oxygenated conditions and bioturbation occurred during regressions (Page et al., 2007; Yan et al., 2012). It has been suggested that ice sheet growth resulted in enhanced thermohaline circulation and ventilation, while warming and ice melting resulted in increased ocean stratification and anoxia (Page et al., 2007; Yan et al., 2012). In addition, (drivers of) sea level might have affected upwelling and terrestrial influx and therefore primary productivity (e.g., Lu et al., 2019; Page et al., 2007; Zhang, Li, et al., 2022).

6.5. Future research

Integration of our initial cyclostratigraphic framework with published U-Pb ages, sequence stratigraphy, and proxy data provides new insights into the climatic system of the late Ediacaran in the Nama Basin that need to be further explored in future research. Although satellite images are effective for stratigraphic correlations throughout large geographic areas, field studies are needed to further improve the cyclostratigraphic framework by providing detailed information on sedimentology and to identify variations with more accuracy and on a higher resolution. Drone imaging can be used to generate quantitative records of color and weathering profiles, which can be used for statistical analysis like spectral analysis (e.g., Lantink, 2022). To confirm an astronomical origin for the sedimentary alternations, specific stratigraphic intervals need to be targeted for high-precision U-Pb zircon dating of volcanic ash beds, namely intervals that possibly contain hiatuses and intervals that are supposedly continuous, so that cycle durations can be better constrained. This is necessary to be able to distinguish between a dominantly precession-eccentricity or obliquity origin. Subsequently, systematic and high-resolution multi-proxy data must be generated, preferably from fresh rock samples obtained by drilling, and placed in the cyclostratigraphic framework to understand the potential relationship between sea-level change, redox variability, and fossil distribution on astronomical timescales, including their phase relationship. This will provide critical information on the late Ediacaran climate system as well as relative time constraints, ultimately of importance for our understanding of the distribution and evolution of early complex life just prior to the Cambrian Explosion.

7. Conclusion

Satellite images reveal that the middle Nama Group in southern Namibia consists of regular sedimentary alternations that are correlatable throughout the Witputs subbasin over distances of ~50 km. The alternations occur dominantly on scales of several tens of meters, accompanied by smaller- and larger-scale variations in parts of the succession. This allowed for the development of an initial cyclostratigraphic framework based on the most complete stratigraphy. A total of 35 to 39 dominant alternations could be recognized throughout the Nudaus and Urusis Formations in the Witputs subbasin. Integration with published high-precision U-Pb ages resulted in an estimate of ~120–180 k.y. per alternation on the dominant scale. Comparison with the published sequence stratigraphic framework indicates that the dominant alternations are consistent with the medium-scale sequences, which have been interpreted as fluctuations in relative or eustatic sea level (Saylor, 2003).

The estimated cycle duration corresponds well with the period of short eccentricity (~100 k.y.), considering the presence of hiatuses is likely in shallow marine environments. Alternatively, it may correspond with the period of the amplitude modulation of obliquity (~173 k.y.), which would imply no time is missing on this scale. In these cases, the variations on the smaller and larger scales may correspond to precession (~18 k.y.) and long eccentricity (405 k.y.), or obliquity (~30 k.y.) and very long obliquity (~1.2 m.y.), respectively. It is not yet possible to distinguish between these two cyclostratigraphic options as they result in similar cycle ratios and because the availability and uncertainties of the U-Pb ages are insufficient to discriminate between them.

Based on the integrated cyclostratigraphic framework, we hypothesize that astronomically-forced fluctuations in sea level modulated deposition of the Nama Group, most likely through glacio-eustasy or, alternatively, aquifer-eustasy. On the large scale, sedimentation was likely influenced by both astronomical and tectonic processes. Geochemical studies have noted a correlation between fossil distribution, redox changes and sequence stratigraphy in the Nama Group (Wood et al., 2015), suggesting that astronomical forcing possibly played an important role in oxygen availability and in the distribution, or even evolution, of Ediacara biota.

CRediT authorship contribution statement

Bianca R. Spiering: Conceptualization, Methodology, Formal analysis, Investigation, Writing – original draft, Writing – review & editing, Visualization. **Ajani Bissick:** Visualization. **Simon A.F. Darroch:** Writing – review & editing. **Joshua H.F.L. Davies:** Writing – review & editing. **Brandt M. Gibson:** Writing – review & editing. **Galen P. Halverson:** Writing – review & editing. **Marc Laflamme:** Writing – review & editing, Funding acquisition. **Frederik J. Hilgen:** Conceptualization, Writing – review & editing, Supervision, Funding acquisition.

Declaration of Competing Interest

The authors declare that they have no known competing financial interests or personal relationships that could have appeared to influence the work reported in this paper.

Data availability

All data is included in the supplementary material.

Acknowledgements

This work was supported by the Dutch Research Council (NWO; grant number OCENW.M.21.031). We thank B.Z. Saylor for discussion about the sequence stratigraphic framework of the Nama Group.

Appendix A. Supplementary data

Supplementary data to this article can be found online at https://doi.org/10.1016/j.precamres.2023.107200.

References

Blanco, G., Germs, G.J.B., Rajesh, H.M., Chemale Jr., F., Dussin, I.A., Justino, D., 2011. Provenance and paleogeography of the Nama Group (Ediacaran to early Paleozoic, Namibia): Petrography, geochemistry and U-Pb detrital zircon geochronology. Precamb. Res. 187 (1–2), 15–32. https://doi.org/10.1016/j.precamres.2011.02.002.

Boulila, S., Galbrun, B., Miller, K.G., Pekar, S.F., Browning, J.V., Laskar, J., Wright, J.D., 2011. On the origin of Cenozoic and Mesozoic 'third-order' eustatic sequences. Earth Sci. Rev. 109 (3–4), 94–112. https://doi.org/10.1016/j.earscirev.2011.09.003.

Boulila, S., Vahlenkamp, M., de Vleeschouwer, D., Laskar, J., Yamamoto, Y., Pälike, H., Turner, S.K., Sexton, P.F., Westerhold, T., Röhl, U., 2018. Towards a robust and consistent middle Eocene astronomical timescale. Earth Planet. Sci. Let. 486, 94–107. https://doi.org/10.1016/j.epsl.2018.01.003.

Bouougri, E.H., Porada, H., Weber, K., Reitner, J., 2011. Sedimentology and palaeoecology of Ernietta-bearing Ediacaran deposits in southern Namibia: implications for infaunal vendobiont communities. Adv. Stromat. Geobiol. 473–506 https://doi.org/10.1007/978-3-642-10415-2_29.

Bowring, S.A., Grotzinger, J.P., Condon, D.J., Ramezani, J., Newall, M.J., Allen, P.A., 2007. Geochronologic constraints on the chronostratigraphic framework of the Neoproterozoic Huqf Supergroup. Sultanate of Oman. Am. J. Sci. 307 (10), 1097–1145. https://doi.org/10.2475/10.2007.01.

Bowyer, F.T., Shore, A.J., Wood, R.A., Alcott, L.J., Thomas, A.L., Butler, I.B., Curtis, A., Hainanan, S., Curtis-Walcott, S., Penny, A.M., Poulton, S.W., 2020. Regional nutrient decrease drove redox stabilization and metazoan diversification in the late Ediacaran Nama Group, Namibia. Sci. Rep. 10, 2240. https://doi.org/10.1038/s41598-020-59335-2.

Bowyer, F.T., Zhuravlev, A.Y., Wood, R., Shields, G.A., Zhou, Y., Curtis, A., Poulton, S. W., Condon, D.J., Yang, C., Zhu, M., 2022. Calibrating the temporal and spatial dynamics of the Ediacaran-Cambrian radiation of animals. Earth Sci. Rev. 225, 103913 https://doi.org/10.1016/j.earscirev.2021.103913.

Brasier, M., Cowie, J., Taylor, M., 1994. Decision on the Precambrian-Cambrian boundary stratotype. Episodes 17 (1–2), 3–8. https://doi.org/10.18814/epiiugs/1994/v17i1.2/002.

Burns, S.J., Matter, A., 1993. Carbon isotope record of the latest Proterozoic from Oman. Eclogae Geol. Helvetiae 86 (2), 595–607. https://doi.org/10.5169/seals-167254.

Catuneanu, O., Beaumont, C., Waschbusch, P., 1997. Interplay of static loads and subduction dynamics in foreland basins: Reciprocal stratigraphies and the 'missing' peripheral bulge. Geol. 25 (12), 1087–1090. https://doi.org/10.1130/0091-7613(1997)025<1087:IOSLAS>2.3.CO;2.

Charbonnier, G., Boulila, S., Spangenberg, J.E., Adatte, T., Föllmi, K.B., Laskar, J., 2018. Obliquity pacing of the hydrological cycle during the Oceanic Anoxic Event 2. Earth Planet. Sci. Lett. 499, 266–277. https://doi.org/10.1016/j.epsl.2018.07.029.

Chen, X., Kuang, H., Liu, Y., Wang, Y., Yang, Z., Vandyk, T.M., Le Heron, D.P., Wang, S., Geng, Y., Bai, H., Peng, N., Xia, X., 2020. Precambr. Res. 334, 105727 https://doi.org/10.1016/j.precamres.2020.105727.
Cherry, L.B., Gilleaudeau, G.J., Grazhdankin, D.V., Romaniello, S.J., Martin, A.J., Kaufman, A.J., 2022. A diverse Ediacara assemblage survived under low-oxygen conditions. Nat. Commun. 13, 7306. https://doi.org/10.1038/s41467-022-35012-y.
Chumakov, N.M., 2011. Late Proterozoic African glacial era. Stratigr. Geol. Correl. 19, 1–20. https://doi.org/10.1134/S0869593810061012.
Cribb, A.T., Kenchington, C.G., Koester, B., Gibson, B.M., Boag, T.H., Racicot, R.A., Mocke, H., Laflamme, M., Darroch, S.A.F., 2019. Increase in metazoan ecosystem engineering prior to the Ediacaran-Cambrian boundary in the Nama Group, Namibia. R. Soc. Open Sci. 6, 190548 https://doi.org/10.1098/rsos.190548.
Daher, H., Arbic, B.K., Williams, J.G., Ansong, J.K., Boggs, D.H., Müller, M., Schindelegger, M., Austermann, J., Cornuelle, B.D., Crawford, E.B., Fringer, O.B., Lau, H.C.P., Lock, S.J., Maloof, A.C., Menemenlis, D., Mitrovica, J.X., Green, J.A.M., Huber, M., 2021. Long-term Earth-Moon evolution with high-level orbit and ocean tide models. J. Geophys. Res. Plan. 126(12), e2021JE006875.
Darroch, S.A.F., Sperling, E.A., Boag, T.H., Racicot, R.A., Mason, S.J., Morgan, A.S., Tweedt, S., Myrow, P., Johnston, D.T., Erwin, D.H., Laflamme, M., 2015. Biotic replacement and mass extinction of the *Ediacara biota*. Proc. R. Soc. B 282 (1814), 20151003. https://doi.org/10.1098/rspb.2015.1003.
Darroch, S.A.F., Cribb, A.T., Buatois, L.A., Germs, G.J.B., Kenchington, C.G., Smith, E.F., Mocke, H., O'Neil, G.R., Schiffbauer, J.D., Maloney, K.M., Racicot, R.A., Turk, K.A., Gibson, B.M., Almond, J., Koester, B., Boag, T.H., Tweedt, S.M., Laflamme, M., 2021. The trace fossil record of the Nama Group, Namibia: exploring the terminal Ediacaran roots of the Cambrian explosion. Earth Sci. Rev. 212, 103435 https://doi.org/10.1016/j.earscirev.2020.103435.
Davies, A., Gréselle, B., Hunter, S.J., Baines, G., Robson, C., Haywood, A.M., Ray, D.C., Simmons, M.D., Buchem, F.S.P., 2020. Assessing the impact of aquifer-eustasy on short-term Cretaceous sea-level. Cretac. Res. 112, 104445 https://doi.org/10.1016/j.cretres.2020.104445.
Davydov, V.I., Crowley, J.L., Schmitz, M.D., Poletaev, V.I., 2010. High-precision U-Pb zircon age calibration of the global Carboniferous time scale and Milankovitch band cyclicity in the Donets Basin, eastern Ukraine. Geochem. Geophys. Geosyst. 11 (2), Q0AA04. https://doi.org/10.1029/2009GC002736.
Erwin, D.H., Laflamme, M., Tweedt, S.M., Sperling, E.A., Pisani, D., Peterson, K.J., 2011. The Cambrian conundrum: Early divergence and later ecological success in the early history of animals. Sci. 334 (6059), 1091–1097. https://doi.org/10.1126/science.1206375.
Evans, S.D., Tu, C., Rizzo, A., Surprenant, R.L., Boan, P.C., McCandless, H., Marshall, N., Xiao, S., Droser, M.L., 2022. Environmental drivers of the first major animal extinction across the Ediacaran White Sea-Nama transition. Proc. Natl. Acad. Sci. 119 (46) https://doi.org/10.1073/pnas.2207475119.
Fang, J., Wu, H., Fang, Q., Shi, M., Zhang, S., Yang, T., Li, H., Cao, L., 2020. Cyclostratigraphy of the global stratotype section and point (GSSP) of the basal Guzhangian Stage of the Cambrian Period. Palaeogeogr. Palaeoclimatol. Palaeoecol. 540, 109530 https://doi.org/10.1016/j.palaeo.2019.109530.
Farhat, M., Auclair-Desrotour, P., Boué, G., Laskar, J., 2022. The resonant tidal evolution of the Earth-Moon distance. A & A 665, L1. https://doi.org/10.1051/0004-6361/202243445.
García, A., Segura, M., García-Hidalgo, J.F., 1996. Sequences, cycles and hiatuses in the Upper Albian-Cenomanian of the Iberian Ranges (Spain): a cyclostratigraphic approach. Sedimentary Geol. 103 (3–4), 175–200. https://doi.org/10.1016/0037-0738(95)00109-3.
Germs, G.J.B., 1983. Implications of a sedimentary facies and depositional environmental analysis of the Nama Group in south west Africa/Namibia. In: Miller, R.M. (Ed.), Evolution of the Damara Orogen of South West Africa/Namibia, vol. 11. Special Publications, Geological Society of South Africa, Johannesburg, pp. 89–114.
Germs, G.J.B., Gaucher, C., 2012. Nature and extent of a late Ediacaran (ca. 547 Ma) glacigenic erosion surface in southern Africa. S. Afr. J. Geol. 115 (1), 91–102. https://doi.org/10.2113/gssajg.115.91.
Germs, G.J.B., Gresse, P.G., 1991. The foreland basin of the Damara and Gariep orogens in Namaqualand and southern Namibia: stratigraphic correlations and basin dynamics. S. Afr. J. Geol. 94 (2–3), 159–169.
Germs, G.J.B., Miller, R.M., Frimmel, H.E., Gaucher, C., 2009. Syn- to late-orogenic sedimentary basins of southwestern Africa. In: Gaucher, C., Sial, A.N., Halverson, G. P., Frimmel, H.E. (Eds.), Neoproterozoic-Cambrian Tectonics, Global Change and Evolution: A Focus on South Western Gondwana. Developments in Precambrian Geology, vol. 16. Elsevier, pp. 183–203. https://doi.org/10.1016/S0166-2635(09)01613-2.
Gong, Z., Li, M., 2020. Astrochronology of the Ediacaran Shuram carbon isotope excursion. Oman. Earth Planet. Sci. Lett. 547, 116462 https://doi.org/10.1016/j.epsl.2020.116462.
Gray, D.R., Foster, D.A., Meert, J.G., Goscombe, B.D., Armstrong, R., Trouw, R.A.J., Passchier, C.W., 2008. A Damara orogen perspective on the assembly of southwestern Gondwana. In: Pankhurst, R.J., Trouw, R.A.J., Brito Neves, B.B., de Wit, M.J. (Eds.), West Gondwana: Pre-Cenozoic Correlations Across the South Atlantic Region. Geological Society, London, Special Publications, vol. 294, pp. 257–278. 10.1144/SP294.14.
Gresse, P.G., Germs, G.J.B., 1993. The Nama foreland basin: sedimentation, major unconformity bounded sequences and multisided active margin advance. Precambr. Res. 63 (3–4), 247–272. https://doi.org/10.1016/0301-9268(93)90036-2.
Grotzinger, J.P., Bowring, S.A., Saylor, B.Z., Kaufman, A.J., 1995. Biostratigraphic and geochronologic constraints on early animal evolution. Sci. 270 (5236), 598–604. https://doi.org/10.1126/science.270.5236.598.
Grotzinger, J.P., Fike, D.A., Fischer, W.W., 2011. Enigmatic origin of the largest-known carbon isotope excursion in Earth's history. Nat. 4, 285–292. https://doi.org/10.1038/ngeo1138.
Hall, M., Kaufman, A.J., Vickers-Rich, P., Ivantsov, A., Trusler, P., Linnemann, U., Hofmann, M., Elliott, D., Cui, H., Fedonkin, M., Hoffmann, K.-H., Wilson, S., Schneider, G., Smith, J., 2013. Stratigraphy, palaeontology and geochemistry of the late Neoproterozoic Aar Member, southwest Namibia: reflecting environmental controls on Ediacara fossil preservation during the terminal Proterozoic in African Gondwana. Precambr. Res. 238, 214–232. https://doi.org/10.1016/j.precamres.2013.09.009.
Haslett, J., Parnell, A., 2008. A simple monotone process with application to radiocarbon-dated depth chronologies. J. R. Stat. Soc. Ser. C. Appl. Stat. 57 (4), 399–418. https://doi.org/10.1111/j.1467-9876.2008.00623.x.
Hinnov, L.A., 2013. Cyclostratigraphy and its revolutionizing applications in the earth and planetary sciences. Geol. Soc. Am. Bull. 125 (11–12), 1703–1734. https://doi.org/10.1130/B30934.1.
Huang, H., Gao, Y., Ma, C., Jones, M.M., Zeeden, C., Ibarra, D.E., Wu, H., Wang, C., 2021. Organic carbon burial is paced by a ~173-ka obliquity cycle in the middle to high latitudes. Sci. Adv. 7 (28), eabf9489. https://doi.org/10.1126/sciadv.abf9489.
Imbrie, J., Imbrie, J.Z., 1980. Modeling the climatic response to orbital variations. Sci. 207 (4434), 943–953. https://doi.org/10.1126/science.207.4434.943.
Kaufman, A.J., Hayes, J.M., Knoll, A.H., Germs, G.J.B., 1991. Isotopic compositions of carbonates and organic carbon from upper Proterozoic successions in Namibia: stratigraphic variation and the effects of diagenesis and metamorphism. Precambr. Res. 49 (3–4), 301–327. https://doi.org/10.1016/0301-9268(91)90039-D.
Lantink, M.L., Davies, J.H.F.L., Ovtcharova, M., Hilgen, F.J., 2022. Milankovitch cycles in banded iron formations constrain the Earth-Moon system 2.46 billion years ago. Proc. Natl. Acad. Sci. 119(40), e 2117146119. 10.1073/pnas.2117146119.
Lantink, M.L., Lenstra, W.K., Davies, J.H.F.L., Hennekam, R., Martin, D.M., Mason, P.R. D., Reichart, G.-J., Slomp, C.P., Hilgen, F.J., 2023. Precessional pacing of early Proterozoic redox cycles. Earth Planet. Sci. Lett. 610, 118117 https://doi.org/10.1016/j.epsl.2023.118117.
Lantink, M.L., 2022. Milankovitch cycles in banded iron formations: An early Paleoproterozoic window into Earth's climate and Solar System evolution. Utrecht Studies in Earth Sciences 257 (Dissertation). 10.33540/1411.
Laskar, J., Joutel, F., Robutel, P., 1993. Stabilization of the Earth's obliquity by the Moon. Nature 361, 615–617. https://doi.org/10.1038/361615a0.
Laskar, J., Fienga, A., Gastineau, M., Manche, H., 2011. La2010: A new orbital solution for the long-term motion of the Earth. A & A 532, A89. https://doi.org/10.1051/0004-6361/201116836.
Levrard, B., Laskar, J., 2003. Climate friction and the Earth's obliquity. Geophys. J. Int. 154 (3), 970–990. https://doi.org/10.1046/j.1365-246X.2003.02021.x.
Li, Z.-X., Evans, D.A.D., Halverson, G.P., 2013. Neoproterozoic glaciations in a revised global palaeogeography from the breakup of Rodinia to the assembly of Gondwanaland. Sed. Geol. 294, 219–232. https://doi.org/10.1016/j.sedgeo.2013.05.016.
Li, C., Shi, W., Cheng, M., Jin, C., Algeo, T.J., 2020. The redox structure of Ediacaran and early Cambrian oceans and its controls. Sci. Bull. 65 (24), 2141–2149. https://doi.org/10.1016/j.scib.2020.09.023.
Liebrand, D., Beddow, H.M., Lourens, L.J., Pälike, H., Raffi, I., Bohaty, S.M., Hilgen, F.J., Saes, M.J.M., Wilson, P.A., van Dijk, A.E., Hodell, D.A., Kroon, D., Huck, C.E., Batenburg, S.J., 2016. Earth Planet. Sci. Lett. 450, 392–405. https://doi.org/10.1016/j.epsl.2016.06.007.
Linnemann, U., Ovtcharova, M., Schaltegger, U., Gärtner, A., Hautmann, M., Geyer, G., Vickers-Rich, P., Rich, T., Plessen, B., Hofmann, M., Zieger, J., Krause, R., Kriesfeld, L., Smith, J., 2019. New high-resolution age data from the Ediacaran-Cambrian boundary indicate rapid, ecologically driven onset of the Cambrian explosion. Terra Nova 31 (1), 49–58. https://doi.org/10.1111/ter.12368.
Linnemann, U., Hofmann, M., Gärtner, A., Gärtner, J., Zieger, J., Krause, R., Haenel, R., Mende, K., Ovtcharova, M., Schaltegger, U., Vickers-Rich, P., 2022. An upper Ediacaran glacial period in Cadomia: the Granville tillite (Armorican Massif) – sedimentology, geochronology and provenance. Geol. Mag. 159 (7), 999–1013. https://doi.org/10.1017/S0016756821001011.
Lisiecki, L.E., Raymo, M.E., 2005. A Pliocene-Pleistocene stack of 57 globally distributed benthic $\delta^{18}O$ records. Paleoceanography 20 (1), PA1003. https://doi.org/10.1029/2004PA001071.
Lu, Y., Huang, C., Jiang, S., Zhang, J., Lu, Y., Liu, Y., 2019. Cyclic late Katian through Hirnantian glacioeustasy and its control of the development of the organic-rich Wufeng and Longmaxi shales, South China. Palaeogeogr. Palaeoclimatol. Palaeoecol. 526, 96–109. https://doi.org/10.1016/j.palaeo.2019.04.012.
Maloney, K.M., Boag, T.H., Facciol, A.J., Gibson, B.M., Cribb, A., Koester, B.E., Kenchington, C.G., Racicot, R.A., Darroch, S.A.F., Laflamme, M., 2020. Paleoenvironmental analysis of Ernietta-bearing Ediacaran deposits in southern Namibia. Palaeogeogr. Palaeoclimatol. Palaeoecol. 556, 109884 https://doi.org/10.1016/j.palaeo.2020.109884.
Matthews, J.J., Liu, A.G., Yang, C., McIlroy, D., Levell, B., Condon, D.J., 2021. A chronostratigraphic framework for the rise of the Ediacaran macrobiota: new constraints from mistaken point ecological reverse, Newfoundland. GSA Bull. 133 (3/4), 612–624. https://doi.org/10.1130/B35646.
Meyers, S.R., Malinverno, A., 2018. Proterozoic Milankovitch cycles and the history of the solar system. Proc. Natl. Acad. Sci. 115 (25), 6363–6368. https://doi.org/10.1073/pnas.1717689115.
Miller, K.G., Kominz, M.A., Browning, J.V., Wright, J.D., Mountain, G.S., Katz, M.E., Sugarman, P.J., Cramer, B.S., Christie-Blick, N., Pekar, S.F., 2005. The Phanerozoic record of global sea-level change. Sci. 310 (5752), 1293–1298. https://doi.org/10.1126/science.1116412.

Narbonne, G.M., Saylor, B.Z., Grotzinger, J.P., 1997. The youngest Ediacaran fossils from southern Africa. J. Paleo. 71 (6), 953–967. https://doi.org/10.1017/S0022336000035940.

Naylor, M., Sinclair, H.D., 2007. Punctuated thrust deformation in the context of doubly vergent thrust wedges: Implications for the localization of uplift and exhumation. Geol. 35 (6), 559–562. https://doi.org/10.1130/G23448A.1.

Nelson, L.L., Ramezani, J., Almond, J.E., Darroch, S.A.F., Taylor, W., Brenner, D.C., Furey, R.P., Turner, M., Smith, E.F., 2022. Pushing the boundary: a calibrated Ediacaran-Cambrian stratigraphic record from the Nama Group in northwestern Republic of South Africa. Earth Planet. Sci. Lett. 580, 117396 https://doi.org/10.1016/j.epsl.2022.117396.

Olsen, P.E., Laskar, J., Kent, D.V., Kinney, S.T., Reynolds, D.J., Sha, J., Whiteside, J.H., 2019. Mapping solar system chaos with the geological orrery. Proc. Natl. Acad. Sci. 116 (22), 10664–10673. https://doi.org/10.1073/pnas.1813901116.

Page, A.A., Zalasiewicz, J.A., Williams, M., Popov, L.E., 2007. Were transgressive black shales a negative feedback modulating glacioeustasy in Early Paleozoic Icehouse? In: Williams, M., Haywood, A.M., Gregory, F.J., Schmidt, D.N. (Eds.), Deep-time Perspectives on Climate Change: Marrying the Signal from Computer Models and Biological Proxies. The Micropalaeontological Society, Special Publications, the Geological Society, London, pp. 123–156.

Pu, J.P., Bowring, S.A., Ramezani, J., Myrow, P., Raub, T.D., Landing, E., Mills, A., Hodgin, E., Macdonald, F.A., 2016. Dodging snowballs: Geochronology of the Gaskiers glaciation and the first appearance of the *Ediacaran biota*. Geol. 44 (11), 955–958. https://doi.org/10.1130/G38284.1.

Ries, J.B., Fike, D.A., Pratt, L.M., Lyons, T.W., Grotzinger, J.P., 2009. Superheavy pyrite ($\delta^{34}S_{pyr} > \delta^{34}S_{CAS}$) in the terminal Proterozoic Nama Group, southern Namibia: a consequence of low seawater sulfate at the dawn of animal life. Geology 37 (8), 743–746. https://doi.org/10.1130/G25775A.1.

Rose, C., Prave, T., Baillie, I., Cantine, M., Kasemann, S., Macdonald, F., Mesli, M., Nduutepo, A., Pruss, S., Trindade, R., Zhu, M., 2023. Grinding through the Ediacaran-Cambrian Transition (EGU23-9523). EGU General Assembly 2023, Vienna, Austria. 10.5194/egusphere-egu23-9523.

Saylor, B.Z., 2003. Sequence stratigraphy and carbonate-siliciclastic mixing in a terminal Proterozoic foreland basin, Urusis Formation, Nama Group. Namibia. J. Sediment. Res. 73 (2), 264–279. https://doi.org/10.1306/082602730264.

Saylor, B.Z., Grotzinger, J.P., Germs, G.J.B., 1995. Sequence stratigraphy and sedimentology of the Neoproterozoic Kuibis and Schwarzrand Subgroups (Nama Group), southwestern Namibia. Precambr. Res. 73 (1–4), 153–171. https://doi.org/10.1016/0301-9268(94)00076-4.

Saylor, B.Z., Kaufman, A.J., Grotzinger, J.P., Urban, F., 1998. A composite reference section for terminal Proterozoic strata of southern Namibia. J. Sediment. Res. 68 (6), 1223–1235. https://doi.org/10.2110/jsr.68.1223.

Saylor, B.Z., Poling, J.M., Huff, W.D., 2005. Stratigraphic and chemical correlation of volcanic ash beds in the terminal Proterozoic Nama Group. Namibia. Geol. Mag. 142 (5), 519–538. https://doi.org/10.1017/S0016756805000932.

Sørensen, A.L., Nielsen, A.T., Thibault, N., Zhao, Z., Schovsbo, N.H., Dahl, T.W., 2020. Astronomically forced climate change in the late Cambrian. Earth Planet. Sci. Lett. 548, 116475 https://doi.org/10.1016/j.epsl.2020.116475.

Sperling, E.A., Wolock, C.J., Morgan, A.S., Gill, B.C., Kunzmann, M., Halverson, G.H., Macdonald, F.A., Knoll, A.H., Johnston, D.T., 2015. Statistical analysis of iron geochemical data suggests limited late Proterozoic oxygenation. Nat. 523, 451–454. https://doi.org/10.1038/nature14589.

Tostevin, R., Bradbury, H.J., Shields, G.A., Wood, R.A., Bowyer, F., Penny, A.M., Turchyn, A.V., 2019a. Calcium isotopes as a record of the marine calcium cycle versus carbonate diagenesis during the late Ediacaran. Chem. Geol. 529, 119319 https://doi.org/10.1016/j.chemgeo.2019.119319.

Tostevin, R., Clarkson, M., Gangl, S., Shields, G.A., Wood, R.A., Bowyer, F., Penny, A.M., Stirling, C.H., 2019b. Uranium isotope evidence for an expansion of anoxia in terminal Ediacaran oceans. Earth Planet. Sci. Lett. 506, 104–112. https://doi.org/10.1016/j.epsl.2018.10.045.

Tostevin, R., Mills, B.J.W., 2020. Reconciling proxy records and models of Earth's oxygenation during the Neoproterozoic and Paleozoic. Interface Focus 10 (4), 20190137. https://doi.org/10.1098/rsfs.2019.0137.

Tostevin, R., Wood, R.A., Shields, G.A., Poulton, S.W., Guilbaud, R., Bowyer, F., Penny, A.M., He, T., Curtis, A., Hoffmann, K.H., Clarkson, M.O., 2016. Low-oxygen waters limited habitable space for early animals. Nat. Commun. 7, 12818. https://doi.org/10.1038/ncomms12818.

Tostevin, R., He, T., Turchyn, A.V., Wood, R.A., Penny, A.M., Bowyer, F., Antler, G., Shields, G.A., 2017. Constraints on the late Ediacaran sulfur cycle from carbonate associated sulfate. Precambr. Res. 290, 113–125. https://doi.org/10.1016/j.precamres.2017.01.004.

Vickers-Rich, P., Ivantsov, A.Y., Trusler, P.W., Narbonne, G.M., Hall, M., Wilson, S.A., Greentree, C., Fedonkin, M.A., Elliott, D.A., Hoffmann, K.H., Schneider, G.I.C., 2013. Reconstructing Rangea: New discoveries from the Ediacaran of southern Namibia. J. Paleo. 87 (1), 1–15. https://doi.org/10.1666/12-074R.1.

Waltham, D., 2015. Milankovitch period uncertainties and their impact on cyclostratigraphy. J. Sediment. Res. 85 (8), 990–998. https://doi.org/10.2110/jsr.2015.66.

Wang, R., Shen, B., Lang, X., Wen, B., Mitchell, R.N., Ma, H., Yin, Z., Peng, Y., Liu, Y., Zhou, C., 2023. A great late Ediacaran ice age. Natl. Sci. Rev. 10 (8), nwad117 https://doi.org/10.1093/nsr/nwad117.

Wang, W., Zhou, C., Guan, C., Yuan, X., Chen, Z., Wan, B., 2014. An integrated carbon, oxygen, and strontium isotopic studies of the Lantian Formation in South China with implications for the Shuram anomaly. Chem. Geol. 373, 10–26. https://doi.org/10.1016/j.chemgeo.2014.02.023.

Webb, D.J., 1982. Tides and the evolution of the Earth-Moon system. Geophys. J. Int. 70 (1), 261–271. https://doi.org/10.1111/j.1365-246X.1982.tb06404.x.

Wei, G.-Y., Planavsky, N.J., He, T., Zhang, F., Stockey, R.G., Cole, D.B., Lin, Y.-B., Ling, H.-F., 2021. Global marine redox evolution from the late Neoproterozoic to the early Paleozoic constrained by the integration of Mo and U isotope records. Earth Sci. Rev. 214, 103606 https://doi.org/10.1016/j.earscirev.2021.103506.

Wendler, J.E., Wendler, I., 2016. What drove sea-level fluctuations during the mid-Cretaceous greenhouse climate? Palaeogeogr. Palaeoclimatol. Palaeoecol. 441, 412–419. https://doi.org/10.1016/j.palaeo.2015.08.029.

Wendler, J.E., Wendler, I., Vogt, C., Kuss, J., 2016. Link between cyclic eustatic sea-level change and continental weathering: Evidence for aquifer-eustasy in the Cretaceous. Palaeogeogr. Palaeoclimatol. Palaeoecol. 441, 430–437. https://doi.org/10.1016/j.palaeo.2015.08.014.

Williams, G.E., 1993. History of the Earth's obliquity. Earth Sci. Rev. 34 (1), 1–45. https://doi.org/10.1016/0012-8252(93)90004-Q.

Williams, D.M., Kasting, J.F., Frakes, L.A., 1998. Low-latitude glaciation and rapid changes in the Earth's obliquity explained by obliquity-oblateness feedback. Nat. 396, 453–455. https://doi.org/10.1038/24845.

Wilson, J.P., Grotzinger, J.P., Fischer, W.W., Hand, K.P., Jensen, S., Knoll, A.H., Abelson, J., Metz, J.M., McLoughlin, N., Cohen, P.A., Tice, M.M., 2012. Deep-water incised valley deposits at the Ediacaran-Cambrian boundary in southern Namibia contain abundant Treptichnus pedum. PALAIOS 27 (4), 252–273. https://doi.org/10.2110/palo.2011.p11-036r.

Wood, R., Erwin, D.H., 2018. Innovation not recovery: Dynamic redox promotes metazoan radiations. Biol. Rev. 93 (2), 863–873. https://doi.org/10.1111/brv.12375.

Wood, R., Liu, A.G., Bowyer, F., Wilby, P.R., Dunn, F.S., Kenchington, C.G., Cuthill, J.F. H., Mitchell, E.G., Penny, A., 2019. Integrated records of environmental change and evolution challenge the Cambrian Explosion. Nat. Ecol. Evol. 3, 528–538. https://doi.org/10.1038/s41559-019-0821-6.

Wood, R.A., Poulton, S.W., Prave, A.R., Hoffmann, K.-H., Clarkson, M.O., Guilbaud, R., Lyne, J.W., Tostevin, R., Bowyer, F., Penny, A.M., Curtis, A., Kasemann, S.A., 2015. Dynamic redox conditions control late Ediacaran metazoan ecosystems in the Nama Group. Namibia. Precambrian Res. 261, 252–271. https://doi.org/10.1016/j.precamres.2015.02.004.

Yan, D., Chen, D., Wang, Q., Wang, J., 2012. Predominance of stratified anoxic Yangtze Sea interrupted by short-term oxygenation during the Ordo-Silurian transition. Chem. Geol. 291, 69–78. https://doi.org/10.1016/j.chemgeo.2011.09.015.

Zhang, Z., Huang, Y., Li, M., Li, X., Ju, P., Wang, C., 2022b. Obliquity-forced aquifer-eustasy during the Late Cretaceous greenhouse world. Earth Planet. Sci. Lett. 596, 117800 https://doi.org/10.1016/j.epsl.2022.117800.

Zhang, T., Li, Y., Fan, T., Da Silva, A.-C., Shi, J., Gao, Q., Kuang, M., Liu, W., Gao, Z., Li, M., 2022a. Orbitally-paced climate change in the early Cambrian and its implications for the history of the Solar System. Earth Planet. Sci. Lett. 583, 117420 https://doi.org/10.1016/j.epsl.2022.117420.

Zhang, F., Xiao, S., Romaniello, S.J., Hardisty, D., Li, C., Melezhik, V., Pokrovsky, B., Cheng, M., Shi, W., Lenton, T.M., Anbar, A.D., 2019. Global marine redox changes drove the rise and fall of the Ediacara biota. Geobiol. 17 (6), 594–610. https://doi.org/10.1111/gbi.12359.

Zhuravlev, A.Y., Wood, R.A., Bowyer, F.T., 2023. Cambrian radiation speciation events driven by sea level and redoxcline changes on the Siberian Craton. Sci. Adv. 9 (24), eadh2558. https://doi.org/10.1126/sciadv.adh2558.

Xiao, S.H., Narbonne, G.M., 2020. Chapter 18 – The Ediacaran Period. In: Gradstein, F. M., Ogg, J.G., Schmitz, M.D., Ogg, G.M. (Eds.), Geologic Time Scale 2020. Elsevier, vol. 1, pp. 521-561. 10.1016/B978-0-12-824360-2.00018-8.